

Paper size: 8½ x 11”  
Total length: Maximum 4 pages  
Margins: 1” top and bottom, 0.75” left and right  
9 point Times New Roman  
Two Columns

14 point Times New Roman font, no bold or italic, centered, capitalize main words

# Thermal Stability, Grain Growth Kinetics and Mechanical Properties of Bulk Ultrafine Grained AA6063/SiC Composites with Varying Reinforcement Size

O.B. Bembalge\*, S.K. Panigrahi\*

<sup>1</sup>Department of Mechanical Engineering

Indian Institute of Technology Madras, Chennai- 600036, India

Email: email of Presenting Author/Corresponding Author\*

10 point Times New Roman, bold on Author Name, centered

## ABSTRACT

Bulk ultrafine-grained (UFG) AA6063/4wt%SiC composites with varying reinforcement sizes (12 µm (coarse), 1 µm (fine), 45 nm (nano)) have been developed by a hybrid route of stir-casting and cryorolling. In the present work, the influence of annealing temperatures (423 K to 573 K) on the precipitation evolution, particle stimulated nucleation (PSN), recrystallization, grain growth kinetics and thermal stability of developed bulk UFG composites have been studied, and the resultant effect of microstructural evolution is correlated with mechanical properties. UFG coarse and UFG fine composites have shown evidence of recrystallized grains via PSN and retained their UFG microstructure up to 473 K and 523 K, respectively. Superior microstructural stability with retained UFG microstructure up to 573 K was observed in the UFG nanocomposite due to the effective pinning of nano SiC particles and precipitates along grain boundaries. This ultimately resulted in increased grain growth activation energy and strength of the UFG nanocomposite. However, the overall increase in strength is maximum in the UFG nanocomposite due to the dominant effect of dislocation strengthening, grain boundary strengthening and precipitation strengthening mechanisms. A thorough examination of the microstructural evolution of UFG composites at different annealing temperatures along with their mechanical behavior is presented in this paper.

**Keywords:** Metal matrix composite, ultrafine-grained material, thermal stability, particle stimulated nucleation.

## 1. INTRODUCTION

The development of bulk ultrafine-grained (UFG) metal matrix composites (MMC) is compared with coarse-grained counterparts. Among UFG MMCs, UFG particulate aluminum metal matrix composites (AMMC) have drawn considerable attention in academic research and industrial applications [2,3]. Severe plastic deformation (SPD) methods are being extensively used to develop bulk UFG composites. Accumulative roll bonding (ARB) [4,5], equal channel angular pressing (ECAP) [6], high-pressure torsion (HPT) [7], and friction stir processing (FSP) [8,9] are well-established SPD techniques used to develop bulk UFG composites. These deformation techniques store a high fraction of dislocation density in the matrix, refine the microstructure in the UFG/NS regime and hence impart extraordinary properties to UFG composites. SPD-processed materials often possess high stored energy. However, this stored energy in UFG/NS composites may lead to high thermal instability and make the microstructure unstable [10-13]. When such composites with UFG/NS grains are subjected to thermal cycles, they have the tendency to minimize the energy for grain growth by decreasing the grain boundary area and result in loss of UFG/NS structure [14]. Furthermore, in addition to the UFG/NS grain structure, the SPD-processed composite materials also possess fine dislocation structures with a large number of stored dislocations [15]. The density of dislocation changes with a reduction in reinforcement particle size [16]. The dislocation structures are even highly thermally unstable compared to the grain structures developed by various SPD techniques [4-18]. Therefore, the thermal stability of UFG composite materials developed by any

SPD process should be thoroughly examined before considering them for any engineering application.

## 2. EXPERIMENTAL METHOD

In the present work, a commercially available AA6063 alloy was used as a matrix and three different sizes of α-SiC particles (in polycrystalline form) were used as reinforcement. The major alloying elements of the matrix alloy (AA6063) are particles were sizes of 12 µm, coarse, fine and nano, respectively.

**Table 1:** Major alloying elements of the AA6063 alloy.

Element	Mg	Si	Cr	Cu	Fe	Mn	Zn	Ti	Al
Wt.%	0.89	0.54	0.08	0.09	0.22	0.03	0.08	0.01	Rest

In the first stage, individual plates of coarse, fine and nano SiC particles reinforced into the AA6063 matrix were developed via a stir-casting process. A bottom-pouring stir-casting furnace was used to melt the AA6063 alloy at 923 K temperature. At this temperature, stirring was performed for 5 to 10 min to create a semisolid melt alloy vortex. The capsules of SiC powders wrapped in aluminum foil were added into a semisolid melt alloy vortex. The mixture of semisolid alloy and SiC powder was then stirred by a two-stage stirrer at 500 rpm for 10 min. To increase the fluidity of the composite mixture, the temperature was raised to 973 K and maintained for 10 min. The bottom pouring arrangement was used to pour the molten mixture of alloy and SiC powder into the die of size 300×100×11 mm<sup>3</sup>. The same method was used to cast all three

types of composites, followed by partial rolling to 20% to remove the porosity.

### 3. RESULTS

#### 3.1 XRD analysis

XRD analysis of as-cast, solution treated and cryorolled composite materials at different annealing temperatures (423 K, 473 K, 523 K and 573 K) is shown in Fig. 1. The XRD results of as-cast, solution treated and cryorolled composites and their comparative studies were reported in the author's previous work [16,30]. In the present study, at an annealing temperature of 423 K, no significant changes in XRD maps were observed in the UFGB and UFG composite materials. However, a low-intensity peak of the Mg<sub>2</sub>Si precipitate was observed after an annealing temperature of 473 K in all UFG materials. The peak intensity of the Mg<sub>2</sub>Si precipitate increased at 523 K and 573 K annealing temperatures, and the peaks of AlCuMgSi and AlFeSi precipitates were observed at these temperatures in the UFGB and UFG composite materials (Fig. 1 a, b, c & d).

Level 2 headline: 9 point  
Times New Roman Bold

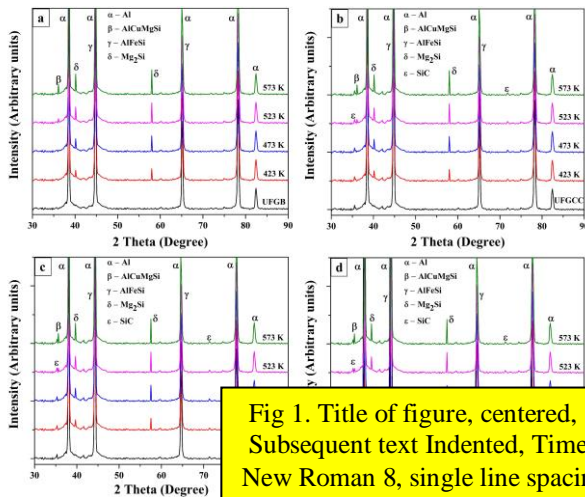


Fig 1. Title of figure, centered,  
Subsequent text Indented, Times  
New Roman 8, single line spacing

**Fig. 1** — XRD profiles of (a) UFGB, (b) UFGCC, (c) UFGFC and (d) UFGNC subjected to different annealing temperatures for 1 hour.

#### 3.2 Microstructural evolution of UFG materials after annealing

The microstructural evolution of UFG materials after annealing in the temperature range of 423 K to 573 K for 1 hour was analyzed by TEM and EBSD. The deformed and annealed microstructures contained dislocated cell structures, subgrains, ultrafine grains (UFG), and particle stimulated nucleation (PSN) in regions surrounding the SiC particles and precipitates, which are represented in the figure by thin yellow arrows, thick yellow arrows, unfilled yellow arrows, yellow dotted circles and red thin arrows, respectively. Fig. 3 shows the deformed microstructure of the UFG base and UFG composite materials before annealing. The UFGB microstructure showed a high density of dislocation along with dislocated cell structures of 150±50 nm (Fig. 3a). The UFGCC consisted of densely packed dislocations in regions surrounding coarse SiC particles and dislocation cells (125±50 nm) in the matrix region away from SiC particles (Fig. 3b), which was also reported in the author's previous work [16]. A polygonized cell structure around the SiC particles was observed in the UFGFC (Fig. 3c). The existence of subgrains was also observed in the UFGFC along with the reduced size of dislocated cell structure (90±25 nm) compared to the UFGCC. The UFGNC microstructure (Fig. 3d) appeared

to be heavily packed with dislocations. The dislocation cell structures and subgrains in the UFGNC (80±20 nm) were found to be in the nanoscale range, smaller than those of the UFGCC and UFGFC materials. Prior to annealing at different temperatures, the presence of secondary compounds (such as Al<sub>4</sub>C<sub>3</sub>) located at the interface of the Al-SiC was quantified based on TEM and XRD analysis to understand their effect on microstructural evolution. The TEM micrographs of the UFGCC (Fig. 3b), UFGFC (Fig. 3c) and UFGNC (Fig. 3d) showed the interdiffusion of Al-SiC without any secondary compound/intermetallic formation (such as Al<sub>4</sub>C<sub>3</sub>). These results were also validated with XRD (Fig. 1) analysis, which showed no evidence of secondary compound formation such as Al<sub>4</sub>C<sub>3</sub>. These UFG composites were then annealed at various temperatures from 423 K to 573 K to understand their microstructural evolution.

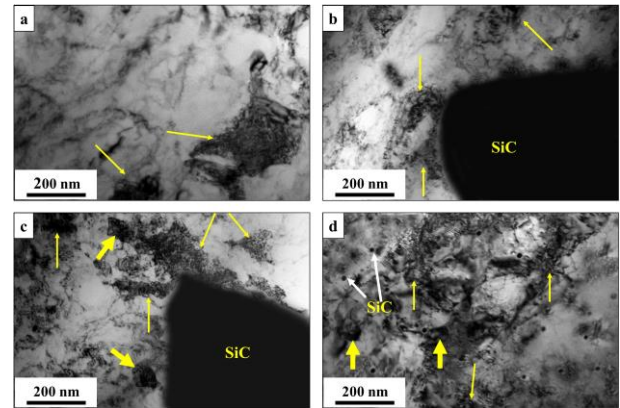


**Fig. 3** — TEM micrographs of (a) UFGB, (b) UFGCC, (c) UFGFC and (d) UFGNC in cryorolled conditions.

EBSD analysis was performed to examine the evolution of microstructure during annealing at temperatures ranging from 423 K to 573 K. In EBSD images, RD and TD represent the rolling and transverse directions, respectively, whereas the thickness direction (normal direction ND) is perpendicular to the paper (not shown in figures). EBSD micrographs of the UFGB, UFGCC, UFGFC and UFGNC before annealing are shown in Fig. 8. The black and red lines in the microstructure indicate the location of high angle grain boundaries (HAGB) (≥ 15°) and low angle grain boundaries (LAGB) (2°-15°), respectively. EBSD micrographs of the UFGB and UFG composite materials exhibit severely fragmented grains (Fig. 8). It can be observed from the figure that the microstructure of all UFG materials is dominated by LAGBs (Fig. 8 a, b, c & d). In case of UFG composites, the fraction of LAGBs is increased with a decrease in SiC particle size, and these LAGB lines correspond to the dislocation substructures. In the case of the UFGCC (Fig. 8b) and UFGFC (Fig. 8c), the fraction of LAGBs in regions surrounding SiC particles is higher than that in the matrix region. A higher fraction of LAGBs was observed in the UFGNC (Fig. 8d). A kernel average misorientation (KAM) analysis (with the help of EBSD data) was carried out to determine the extent of plastic deformation in UFG materials (Fig. 8). KAM is used to assess the strain induced in the grains of the deformed materials. Recrystallized grains show low KAM values (< 1°), and deformed grains show high (>1°) KAM values [35]. In the present work, KAM values of 1.6695°, 2.4652°, 3.2274° and 3.2671° were obtained for the UFGB, UFGCC, UFGFC and UFGNC, respectively. The higher (>1°) KAM values show highly strained grains in all UFG materials. With a decrease in SiC particle size from coarse to fine to nano,

the KAM values were increased. The UFGNC showed the highest KAM value compared to The UFGB, UFGCC and UFGFC, which indicates that the microstructure possesses highly strained grains.

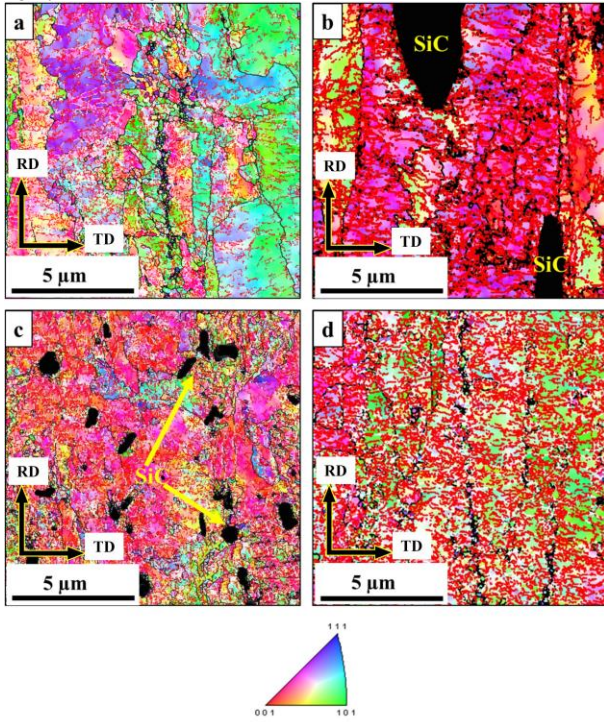


Fig. 8 — EBSD images of (a) UFGB, (b) UFGCC, (c) UFGFC and (d) UFGNC under cryorolled conditions.

### 3.3 Mechanical properties of annealed UFG materials

Table 3 presents the mechanical properties of UFG materials before and after annealing. Fig. 13 shows the tensile test results of the UFGB and UFG composite materials annealed at a temperature range of 423 K to 573 K. A higher strength (ultimate tensile strength (UTS)) was found in the UFGB and UFG composite materials compared to their annealed counterparts, as shown in Table 3. Among all UFG materials, the UFGNC exhibited the maximum UTS (UFGB=275±4 MPa, UFGCC=331±3 MPa, UFGFC=343±2 MPa, UFGNC=409±2 MPa). A small decrease in strength (UTS) along with a slight enhancement in ductility was observed at an annealing temperature of 423 K in the UFGB and UFG composites (Fig. 13 a, b, c & d). A gradual decrease in strength and increase in ductility of the UFGB and UFG composites was observed at 473 K annealing. At annealing temperatures of 523 K and 573 K, a sudden drop in the strength and rise in ductility of the UFGB and UFG composites was observed compared to the 473 K annealing temperature. On the other hand, no significant variations in strength and ductility were observed in all UFG materials at annealing temperatures of 523 K and 573 K.

$$P = \frac{3\gamma V_p}{2d_p}$$

Equations, Justified, 9 point,  
Times New Roman, *Italic*

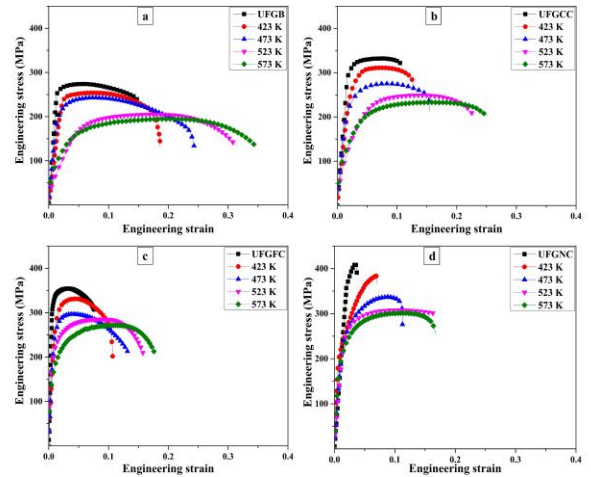


Fig. 13 — Engineering stress-strain curves of (a) UFGB, (b) UFGCC, (c) UFGFC and (d) UFGNC under cryorolled and annealed conditions (at 423 K, 473 K, 523 K and 573 K).

## 4. Discussion

### 4.1 Interface characteristics and precipitation evolution

The interface characteristics and precipitation evolution of the composites are discussed in this section. According to the literature, the interfaces of cast Al/SiC composites often show the formation of secondary compounds such as  $Al_4C_3$  [36]. The formation of secondary compounds is attributed to the interdiffusion of Al and SiC particles. However, evidence for such  $Al_4C_3$ -type intermetallic compound formation has not been observed in the present work (XRD (Fig. 1) and TEM (Fig. 3)). The possible reasons behind the nonoccurrence of secondary compounds (such as  $Al_4C_3$ ) are explained below.

In the present work, the maximum temperature raised during composite casting was 973 K for a short period of time (10 min). During stir-casting, SiC particles were dispersed in liquid aluminum alloy due to the stirring action. The liquid aluminum diffused into SiC at 973 K. This diffusion of Al in SiC during stir-casting was not sufficient to form interdiffusional compounds (such as  $Al_4C_3$ ) because of the much lower duration of holding time (10 min) during casting. Secondary compound ( $Al_4C_3$ ) formation in the Al-SiC system often occurs at a casting temperature of 973 K with a longer holding time ( $\approx 1$  hour) [37-43]. The experimental outcomes of the present study are consistent with the results obtained by Tham et al. [44]. These UFG microstructures without any secondary compounds were used to further examine precipitation evolution.

The precipitation evolution sequence and kinetics were analyzed when the UFGB, UFGCC, UFGFC and UFGNC materials were annealed at various temperatures ranging from 423 K to 573 K. The well-explored precipitation sequence of the AA6063 alloy presented below was used to describe the evolution of precipitates in UFGB, UFGCC, UFGFC and UFGNC materials at various annealing temperatures in the present study [34,45]. The precipitation sequence of the solution-treated AA6063 alloy is as follows:

SSSS (supersaturated solid solution)  $\alpha \rightarrow$  GP zones  $\rightarrow \beta'' \rightarrow \beta' \rightarrow \beta$

The solution treatment of the base alloy (AA6063 alloy) resulted in the complete dissolution of solute atoms into the aluminum matrix and their retainment in a metastable state. Cryorolling the base alloy and composites with varying reinforcement particle sizes at a strain of 2.4 retained the solute atoms in a metastable state (Fig. 3). As the samples were rolled

at cryogenic temperature, they were not supplied with ample energy to evolve the precipitates from solid solution. The spherically shaped GP zones were formed at an annealing temperature of 423 K (Fig. 4 a-d; red arrows). GP zones are clusters of Mg and Si and are clearly visible in the UFGB and UFG composite materials. The GP zones were seen along the boundaries of dislocation cell structures in the UFGFC and UFGNC, as the matrix region was flooded with dislocation cells. Few needle-shaped precipitates ( $\beta''$ ) were observed along with rod-shaped precipitates ( $\beta'$ ) at 473 K annealing in all UFG materials. These rod-shaped precipitates pinned the boundaries of the ultrafine grains and are evident in Fig. 5 a-d. The rod-shaped ( $\beta'$ ) precipitates were dissolved above 473 K annealing, and the stable plate-shaped precipitates ( $\beta$ ) were formed at 523 K annealing. The plate-shaped precipitates were seen along the grain boundaries in the UFGB and UFG composites (Fig. 6 a-d). At 573 K annealing, plate-shaped precipitates were also observed in all UFG materials (Fig. 7 a-d), but the intensity (quantity) of these precipitates was diminished (quantified based on the TEM images of all the UFG materials). Urrutia et al. [46] examined the age-hardening behavior of Al-Mg-Si alloy and observed the formation of  $\beta'$  precipitate at 523 K for 30 min of aging and  $\beta$  precipitate at 523 K for 8 hours of aging. However, in the present work, a similar evolution of various precipitation phases was observed within 523 K in all UFGB and UFG composite materials, even at 1 hour of annealing treatment (much less annealing time compared to 8 hours). This faster precipitation kinetic process was due to the presence of high internal stored energy during cryorolling in the UFGB and UFG composite materials, which provided additional energy for the evolution of precipitates with increasing annealing temperature.

#### 4.2 Thermal stability and grain growth

The annealing of the UFGB and UFG composites led to recovery, recrystallization and grain growth during microstructural evolution. The varying SiC particle size played an important role in the thermal stability and grain growth phenomenon. Reinforcement particle size influenced the recrystallization, grain growth and thermal stability in two dominant ways: particle stimulated nucleation and grain growth retardation (pinning of SiC particles to retard grain growth).

##### 4.2.1 Particle stimulated nucleation

It is well known from previous work [16] that UFG composites have a high dislocation density. The accumulation of (i) severe deformation of the matrix alloy and (ii) mismatch in the thermal expansion coefficient of the matrix alloy and SiC particles. This high density of dislocation in regions surrounding SiC particles creates high strain in the vicinity of SiC particles and acts as an energy pocket. When the UFGCC and UFGFC were annealed at 423 K, the high strain energy and annealing temperature facilitated the driving force for the dislocations accumulated in the vicinity of SiC particles to nucleate and form nano/ultrafine grains in regions surrounding SiC particles (Fig. 4 b & c). This is also called particle-stimulated nucleation (PSN). In case of the UFGNC (Fig. 4d) at 423 K annealing, dislocation cell formation was observed, but there was no evidence of the nucleation of nano/ultrafine grains at the nano SiC particles. This result follows the criterion of minimum particle size, which should be  $\geq 1 \mu\text{m}$  for nucleation of grains developed via PSN as proposed by Humphrey et al. [47]. As per the TEM investigation, nano SiC particles were observed to pin the dislocation cell boundaries in the UFGNC with no sign of PSN

(Figs. 4, 5, 6 & 7). At an annealing temperature of 473 K, the unrecrystallized nano/ultrafine grains evolved and subsequently formed recrystallized UFG grains with clear boundaries near the coarse and fine SiC particles in the UFGCC and UFGFC composites (Fig. 5 b & c). When the UFGCC and UFGFC composites were annealed at 523 K, the strain energy accumulated near the SiC particles due to cryorolling completely recovered and consequently formed fully recrystallized ultrafine grains near the SiC particles (Fig. 6 b & c). At this annealing temperature in the UFGNC, nanoparticles were pinned along the boundaries of UFG grains (Fig. 6d). At an annealing temperature of 573 K, the recrystallized UFG grains (at the periphery of coarse and fine SiC particles) were further developed and subsequently formed grains in the range of  $2 \mu\text{m}$  and  $1 \mu\text{m}$  in regions surrounding the coarse and fine SiC particles, respectively (Fig. 7 b & c).

#### References

- 1 R. Casati, F. Bonollo, D. Dellasega, A. Fabrizi, G. Timelli, A. Tuissi, and M. Vedani: *J. Alloys Compd.*, 2015, vol. 615, pp. S386–8.
- 2 [1] Authors., Journal name, Year, Vol. Page no(s).
- 3 R. Taherzadeh Mousavian, R. Azari Khosroshahi, S. Yazdani, D. Brabazon, and A.F. Boostani: *Mater. Des.*, 2016, vol. 89, pp. 58–70.
- 4 H. Jafarian, J. Habibi-Livar, and S.H. Razavi: *Compos. Part B Eng.*, 2015, vol. 77, pp. 84–92.
- 5 A. Ahmadi, M.R. Toroghnejad, and A. Najafizadeh: *Mater. Des.*, 2014, vol. 53, pp. 13–9.
- 6 A. Hassani and M. Zabihi: *Mater. Des.*, 2012, vol. 39, pp. 140–50.
- 7 H. Asgharzadeh, S.H. Joo, and H.S. Kim: *Metall. Mater. Trans. A*, 2015, vol. 46, pp. 1838–42.
- 8 F. Khan MD and S.K. Panigrahi: *Mater. Sci. Eng. A*, 2016, vol. 675, pp. 338–44.
- 9 F. Khodabakhshi, A.P. Gerlich, A. Simchi, and A.H. Kokabi: *Mater. Sci. Eng. A*, 2014, vol. 620, pp. 471–82.
- 10 R.J. Immanuel and S.K. Panigrahi: *Metall. Mater. Trans. A*, 2017, vol. 48, pp. 3852–68.
- 11 A. Dhal, S.K. Panigrahi, and M.S. Shunmugam: *J. Alloys Compd.*, 2017, vol. 726, pp. 1205–19.
- 12 F. Khan and S.K. Panigrahi: *J. Alloys Compd.*, 2018, vol. 747, pp. 71–82.
- 13 A. Dhal, S.K. Panigrahi, and M.S. Shunmugam: *J. Alloys Compd.*, 2015, vol. 649, pp. 229–38.
- 14 N. Kumar and R.S. Mishra: *Mater. Charact.*, 2012, vol. 74, pp. 1–10.
- 15 N. Gao, M.J. Starink, and T.G. Langdon: *Mater. Sci. Technol.*, 2009, vol. 25, pp. 687–98.
- 16 [18] Authors., "Book title," Edition, Publisher, State, Country, Year, Page no(s).
- 17 2018, vol. 712, pp. 747–56.
- 18 F.J. Humphreys, and M. Hatherly: *Recrystallization and Related Annealing Phenomena*, 2nd ed., Elsevier Ltd., Oxford OX5 1GB, UK, 2004, pp. 1–605.
- 19 M. Balog, T. Hu, P. Krizik, M.V. Castro Riglos, B.D. Saller, H. Yang, J.M. Schoenung, and E.J. Lavernia: *Mater. Sci. Eng. A*, 2015, vol. 648, pp. 61–71.
- 20 S.C. Okumus, S. Aslan, R. Karslioglu, D. Gultekin, and H. Akbulut: *Mater. Sci.*, 2012, vol. 18, pp. 341–6.

Please submit along with Copy right form duly signed